ACS APPLIED POLYMER MATERIALS

pubs.acs.org/acsapm Article

Improving the Mechanical Performance of LDPE/PP Blends through Microfibrillation

Caren Rosales, Nora Aranburu, Itziar Otaegi, Valeria Pettarin, Celina Bernal, Alejandro J. Müller, and Gonzalo Guerrica-Echevarría*

Cite This: https://doi.org/10.1021/acsapm.1c01932 Read Online

ACCESS | Metrics & More | Article Recommendations

ABSTRACT: Polyolefins (polyethylene (PE) and polypropylene (PP)) are the most abundant polymers found in plastic solid waste. They are expensive to separate, and recycling them in the form of blends is not viable due to their immiscibility and incompatibility. Following the idea of the circular economy where waste is turned into raw materials for manufacturing technological products using minimum energy, a solution is proposed for the poor behavior of immiscible PE/PP blends by taking advantage of their immiscibility to transform them into microfibrillar composites (MFCs). PE/PP blends with an 80:20 content ratio were studied, emulating the ratio found in municipal waste. A microfibrillar structure was achieved through an unusual combination of common industrial processing techniques: extrusion, drawing, and injection. The performance of the resulting fibrillar materials was evaluated by means of tensile, fracture, and impact tests, and the results were compared with those of unstretched blends (UBs) with droplet morphology. The effect of adding a compatibilizer was also evaluated. The results were promising as the performance of the MFCs was much better than that of the nonfibrillated blends, and a synergistic effect between the addition of the compatibilizer and microfibrillation process was observed. It seems that this type of processing has great potential for large-scale application in immiscible recycled polyolefin blends in which the final properties can be improved by modifying their morphology, obviating the need to separate these polymers in mixed waste streams.

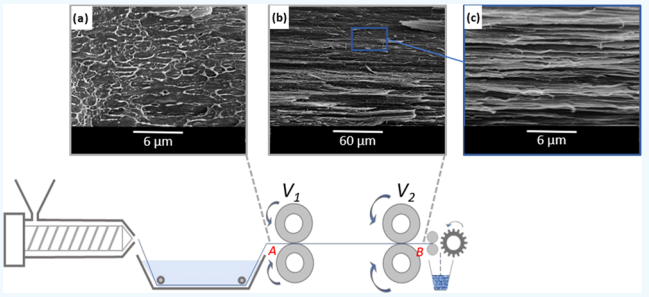

KEYWORDS: *polypropylene, polyethylene, blends, fibrillation, compatibilization, mechanical properties*

1. INTRODUCTION

In recent decades, the significant growth in the world's population has increased the consumption of polymers drastically. In 2018, the global plastics production reached 359 million tons, 36% of which were single-use plastics.[1] Unfortunately, the dramatic growth of the plastics industry has not been accompanied by a recovery strategy, and approximately 91% of plastics are not recycled, resulting in a vast amount of plastic waste and few solutions.

The current production model as a linear economy is not sustainable over time because, without value retention, plastic materials and energy used are wasted. By contrast, the circular economy proposes a new paradigm where waste is converted into raw material for manufacturing new technological products using minimum energy. In this way, waste is reduced, fewer natural resources are extracted, and greenhouse gas emissions are limited.[2−4]

A circular economy requires new technologies for the treatment of waste. Municipal solid waste (MSW) is made up of elements that are discarded after use. Although different percentages of different polymers are found in plastic waste, data published by the UN in 2018[1] reported that polyolefins (polyethylene, PE, and polypropylene, PP), the most abundant polymers in plastic solid waste, account for 70% of the total. The PE/PP ratio in plastic waste was estimated to be somewhere between 80:20 and 65:35 depending on the geographical location.[5]

Developed countries promote the circular economy by obliging companies to use certain amounts of recycled materials in their products. However, two reasons make it difficult to implement large-scale amounts of recycled material: downcycling and the process involved in separating certain plastics from solid waste. In downcycling, the recycled plastic material is of inferior quality and can only be used for other, different applications, thus limiting their "circularity".[6] Second, the process of separating plastic waste into individual polymers is costly and the sorting process is inefficient. One low-cost

Received: December 30, 2021
Accepted: April 21, 2022

separating option could be a simple successive flotation technique that would generate two separate fractions: a light one of low-density polyethylene (LDPE) and PP, and a heavier one, made of the remaining, precipitating plastics.[7,8] Any further separation of LDPE/PP is not economically attractive, so the possibility of recycling them as a blend would seem to be a financially viable alternative.

For some years, blends involving different kinds of PE (LLDPE, LDPE, HDPE),[9−13] and different amounts of PP[14,15] have been studied. These blends have also been compatibilized with a range of copolymers[16−18] and processed using conventional plastic processing methods (injection and compression molding). Mourad et al.[19] provided a thorough insight into how the composition of the blend influences the morphology, the thermal and rheological properties, and, therefore, the mechanical behavior of these materials.[20−25] They concluded that the potential applications of PE and PP are limited, given their immiscibility, incompatibility, and poor interfacial adhesion. In a previous work, blends with different LDPE/PP ratios were studied. It was concluded that the 75:25 LDPE/PP ratio was the most promising blend,[26,27] which also happens to be the same as the PE/PP ratio found in MSW. However, none of these studies provided a solution to the problem of plastic waste. Recently, some isotactic polypropylene (iPP)-polyethylene (PE) multiblock copolymers were synthesized by Xu et al. to use them as compatibilizers.[28] Their results demonstrate exciting opportunities to recycle the world's top two polymers through simple melt blending. However, these copolymers are still at a laboratory scale.

An alternative solution to the poor performance of PE/PP blends would be to take advantage of their immiscibility and transform them into microfibrillar composites (MFCs). MFCs consist of a thermoplastic polymer matrix with microfibrils of another thermoplastic polymer as reinforcement. The blend has to be incompatible for this type of morphology to develop.[29]

The production of MFCs involves three basic steps.[29] The first is a blending stage, where two immiscible polymers (with very different melting temperatures) are melt-blended. The second stage involves hot or cold drawing of the extruded filament, which causes microfibers to develop in both blend components. Finally, a specimen is obtained by injection or compression molding (isotropization) at a processing temperature that lies between the melting temperatures of the two components. This causes the component with the lower melting temperature to melt, forming an isotropic and relaxed MFC matrix. At the same time, microfibers of the higher melting-point component retain their molecular orientation and morphology (without significant changes) and become the reinforcing phase.[29]

In this processing method, a compatibilizer is needed to improve the dispersion of the second phase and the homogeneity of the compound, as it locates at the interface between the two polymers in the blend. In this way, second phase coalescence is avoided and a finer dispersion of smaller particles is achieved. This also leads to enhanced adhesion between phases, which, in turn, allows a more effective load transfer during mechanical loading.[30]

Some work on MFCs has been reported, mostly on PE/PET and PP/PET blends. Yi et al.[31] found that the low viscosity ratio between PP and PET facilitated the formation of smaller and uniformly dispersed particles during the melt blending stage, which led to narrower microfiber diameters after stretching, resulting in greater strength and modulus. Improving the interfacial adhesion led to better mechanical properties than the incompatible system, especially tensile and impact strength. They also studied the exact compatibilizer content above which the mechanical properties are diminished.

Jayanarayanan et al.[32] also studied the PP/PET system and reported that the narrowest PET fibers were obtained with a stretch ratio of 8. Beyond this ratio, fiber breakage was observed during stretching. Consequently, tensile properties improved with the stretch ratio up to an optimized level of between 5 and 8, beyond which they decreased. Furthermore, in a later work,[33] they reported that for some stretch ratios (5 and 8), PET microfibrils can act as heterogeneous nucleation sites for PP crystallization, thus increasing the crystallinity of this phase. In addition, the high aspect ratio (L/D) and abundance of PET microfibrils contributed to delayed thermal degradation, which was not observed at higher stretching ratios.[34] Jayanarayanan et al.[35,36] also studied the LDPE/PET system and reported that the addition of a compatibilizer increased the aspect ratio in LDPE matrix PET fibers. The compatibilized MFCs showed improved mechanical properties (strength and modulus) compared to LDPE (50% higher), blends without a compatibilizer (39%) and blends without stretching (51%). The improvement was not only connected with the presence of the compatibilizer, but the mechanical properties also improved up to 75:25 LDPE/PET blend composition, above which the properties deteriorated as a consequence of fiber agglomeration.

In addition, the diffusivity and permeability of MFCs were found to be lower than those of neat blends due to the tortuous path created for solvent diffusion. Fakirov et al.[37] showed that results obtained for MFCs with LDPE/PET are comparable to those obtained for LDPE with 30% commercial glass fiber, and are even 30 to 40% higher than those following the rule of mixtures. In summary, the aforementioned studies found that there is an inflection point at which mechanical properties no longer improve with the stretching ratio, relative ratio of blends, and compatibilizer content.[36,38−40] To the authors' knowledge, there is no reported work on microfibrillar PE/PP composites obtained by extrusion, stretching, and isotropization.

Based on the aforementioned data, the challenge of this work was to find value in this waste raw material by applying a closed-loop recycling process (upcycling) where the mechanical properties of the material obtained were similar to or even better than those of the original materials.

2. EXPERIMENTAL SECTION

2.1. Materials and Processing. In this study, a low-density polyethylene was used as the matrix (ALCUDIA 2308F, with a melt flow index of 7 g/10 min 2.16 kg, 190 °C) and polypropylene was selected as the minority phase (Isplen PP 070 G2M, with a melt flow index of 12 g/10 min −2.16 kg, 230 °C), both provided by Repsol (Spain). A terpolymer of propylene, ethylene, and butene (Braskem Symbios 4102) was used as a compatibilizer with a melt flow index of 5.5 g/10 min (2.16 kg, 230 °C).

LDPE and PP were manually premixed in an 80:20 weight ratio of LDPE/PP, and the compatibilizer content was set as 0, 7 and 15 wt % of the minority phase, corresponding to 0, 1.4, and 3 wt % of the total PE/PP weight. Melt blending was performed in a Collin ZK 25T SCD15Teach-Line twin-screw extruder (screw diameter = 25 mm, L/D ratio = 18) with a screw speed set to 50 rpm and barrel temperature profile between 160 and 190 °C.

https://doi.org/10.1021/acsapm.1c01932
ACS Appl. Polym. Mater. XXXX, XXX, XXX−XXX

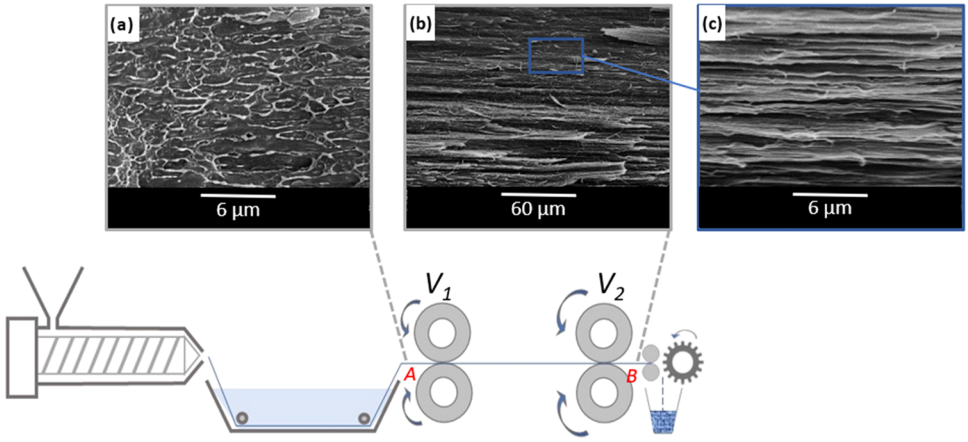

Figure 1. Scheme of the microfibrillation process: unstretched blend (UB) (a) and microfibrillar blend (MFB) at different magnifications (b, c).

Microfibrillar blends (MFB) were obtained immediately after the extrusion process. Figure 1 shows a scheme of the experimental configuration employed. The extruded filament was immersed in a warm water bath at 40 °C for its solidification. This filament was then passed through two pairs of rollers to generate a continuous draw. The first pair of rollers was kept at the same speed as the extrudate and at a temperature of 85 °C. The second pair of rollers was set at a higher speed, to achieve a draw ratio greater than 1. The ratio between the speeds of the two pairs of rollers (V_2/V_1) was taken as the draw ratio and was set equal to 2.5. Immediately after the rolls, the obtained MFB filament was pelletized. In the following stage, the obtained pellets were injection-molded in a Battenfeld BA-230-E machine at 140 °C. This low processing temperature, intermediate between the melting temperature of PE and that of PP, was selected with a view to maintaining the integrity of the PP microfibers and obtaining an MFC. The mold allowed tensile, impact, and fracture test specimens to be obtained in the same cycle. The injection processing parameters were: injection speed: 45 mm/s, injection pressure: 22 MPa, holding time: 3 s, cooling time: 15 s, and the mold was kept at room temperature (23 °C). For comparison purposes, nonstretched blends were extruded and pelletized without applying any stretching step, and then injection-molded with the same processing parameters. The unstretched blends (UBs) were designated in this work as UB-0 (without compatibilizer), UB-7 (with 7% compatibilizer), and UB-15 (with 15% compatibilizer), while the microfibrillated samples were designated as MFC-0, MFC-7, and MFC-15.

2.2. Morphological Characterization. The samples were immersed in liquid nitrogen for 10 min and cryo-fractured to observe the microstructures that developed during processing. All of the cryo-fractured surfaces were coated with a thin layer of gold and observed in a Hitachi S-2700 scanning electron microscope (SEM) with an accelerating voltage of 15 kV. To analyze the effect of the compatibilizer, a quantitative analysis of the morphology of the PP particles in the blends was carried out before stretching. From the SEM micrographs of the unstretched blends, the number and volume average (d_n and d_v) of the cross sections of the particles were measured. For this, Image J software was used to measure at least 300 particles. The size dispersion (D) and the average number of particles per cm^3 were also calculated. The number and volume average were obtained using the following equations[41]

$$d_n = \sum n_i d_i / \sum n_i \tag{1}$$

$$d_v = \sum n_i d_i^4 / \sum n_i d_i^3 \tag{2}$$

where n_i is the number of droplets with diameter d_i.

The particle size polydispersity was evaluated as

$$D = d_v / d_n \tag{3}$$

The volume fraction of the dispersed phase was calculated from the following equation

$$X_v = (X_p/\rho_d)/[X_p/\rho_d + (1 - X_p)/\rho_m] \tag{4}$$

where X_p is the weight fraction of the minority phase, ρ_d is the density of the dispersed phase, and ρ_m is the matrix density.

The mean number of particles per cm^3 was determined from

$$N_i = X_v/[\pi/6(d_n)^3] \tag{5}$$

2.3. Thermal Characterization. A Pyris 7 PerkinElmer under nitrogen atmosphere was used to perform differential scanning calorimetry analysis (DSC). The samples were heated from 50 to 200 °C at 10 °C/min. The percentage crystallinities (Xc_i) of the LDPE and PP in the blends were calculated using the following equation

$$Xc_i = (\Delta H_{m,i}/\Delta H^0_{m,i}\Phi_i) \times 100\% \tag{6}$$

where $\Delta H_{m,i}$ and $\Delta H^0_{m,i}$ are, respectively, the measured melting enthalpies and the heat of fusion for 100% crystalline PE (293 J/g)[31] or PP (207 J/g),[42] and φ_i is the weight fraction of the analyzed constituent.

2.4. Uniaxial Tensile Tests. Tensile tests were carried out following the ASTM D638 standard under quasi-static loading conditions (cross-head speed of 10 mm/min) over dog-bone specimens (type IV) in an Instron universal testing machine (model 5569). Young's modulus (E) was calculated as the maximum slope of the stress−strain curve in the 0.05 and 0.25% strain range. Maximum strength (σ_{max}) and elongation at break (ε_b) were also obtained from the stress−strain curves.

2.5. Fracture Characterization. To evaluate the crack propagation behavior and the toughness of the blends, fracture tests were performed on 80 mm × 12.5 mm SENB specimens (single-edge notched bending) with a thickness of 3.2 mm, under quasi-static loading conditions.

Sharp precracks were introduced perpendicular to the flow direction using a razor blade fitted in a Ceast Notchvis notching machine. Tests were conducted in an Instron EMIC 2350 universal testing machine at room temperature with a constant cross-head speed of 2 mm/min.

To identify the fracture behavior, the concept of ductility level (DL) was applied to exploratory tests using samples with a notch length-to-width ratio (a/W) of 0.5. The DL was defined by Martinez et al.[43] as the relation between the displacement at break and the initial ligament length (l). Five replicates for each blend were tested to ensure result repeatability. The fracture behavior was found to be in the post-yielding range ($0.15 < DL < 1$). The essential work of fracture (EWF) was applied to evaluate the toughness of the materials. EWF is an approach that can be used to evaluate the crack propagation of ductile polymeric materials. This methodology has been extensively used and explained by leading authors on the

https://doi.org/10.1021/acsapm.1c01932
ACS Appl. Polym. Mater. XXXX, XXX, XXX−XXX

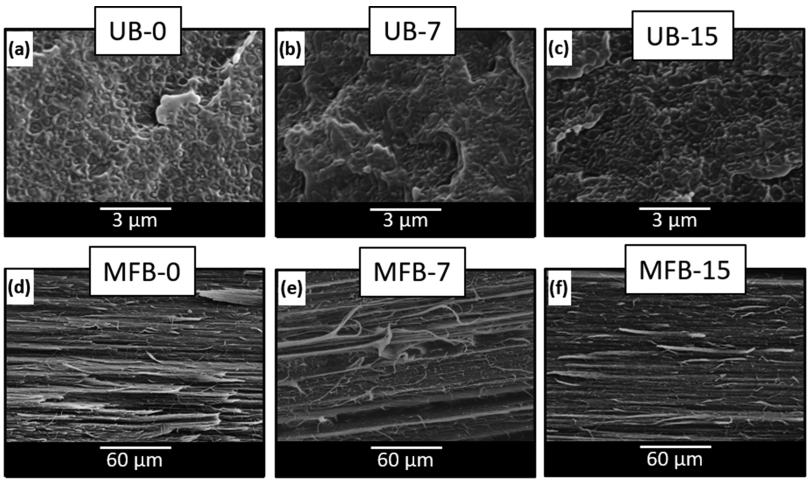

Figure 2. SEM micrographs of the longitudinally cryo-fractured surfaces of extruded LDPE/PP unstretched and microfibrillar blend filaments (UB and MFB, respectively): UB-0 (a), UB-7 (b), UB-15 (c), MFB-0 (d), MFB-7 (e), MFB-15 (f).

subject[43,44] and states that the essential work of fracture, w_f, can be expressed as

$$w_f = W_f/lt = w_e + \beta w_p l \quad (7)$$

where W_f is the total work of fracture, l is the ligament, t is the thickness, β is a geometrical factor, w_e is the essential work of fracture, and w_p is the nonessential work of fracture.

It is important to note that for the plane stress EWF approach to be applicable, it is mandatory that the crack propagates over a fully yielded ligament, and that self-similarity occurs in the load−displacement curves of varying ligament length specimens. The ligament lengths varied between 4 and 12 mm, and the distance between the supports was 72 mm. The fracture surfaces were observed with SEM, under the same conditions used for characterizing the microstructure.

Due to the three-point bending solicitation mode and the considerable ductility of the evaluated materials, some samples did not fracture during the test. Thus, an approach proposed in the literature[45] that suggests using an energy partition between yielding and post-yielding for EWF tests was applied. This partition is applicable for load−displacement curves where the yielding is characteristically separated from the subsequent deformation by a load drop. This point is easily identified in the curve and indicates a clear transition between the onset and the propagation of cracks. The first part indicates the work required for yielding (until the load falls) while the second part indicates the work required for subsequent deformation [eq 8]. In this way, the value $w_{e,y}$ represents the inherent onset parameter of the material. This approach has been successfully applied by several authors[46−48]

$$w_f = w_y + w_n = (w_{e,y} + \beta_y w_{p,y} l) + (w_{e,n} + \beta_n w_{p,n} l) \quad (8)$$

where $w_{e,y}$ and $w_{e,n}$ represent the specific essential works of yielding and subsequent deformation, respectively, and $w_{p,y}$ and $w_{p,n}$ represent the nonessential works of yielding and subsequent deformation, respectively. The values β_y and β_n are geometrical factors associated with the shape of the plastic zone during yielding and subsequent deformation, respectively.

2.6. Impact Characterization. The impact resistance of the materials was studied by Izod impact tests using a CEAST 6548/000 pendulum with an energy of 4 J. Tests were carried out on specimens with a section of 3.2 mm × 12.5 mm obtained by injection molding, in accordance with ASTM D-256 standard recommendations. The notches (2.54 mm depth, 0.25 mm tip radius) were machined after injection molding. A minimum of 8 specimens were tested for each material and the tests were carried out at room temperature (23 °C). The impact resistance was calculated as the ratio between the energy lost by the pendulum through the impact (taking into account the energy lost by friction with the air) and the specimen thickness.

3. RESULTS

3.1. Morphological Characterization. Figure 2 shows the effect of hot drawing on the filament morphology of the MFBs (bottom row) compared with that of the UB filaments (top row). On the one hand, as the figure shows, the hot-drawn material showed the orientation in the form of continuous fibers of both the dispersed phase and the matrix (Figure 2d−f). This fibrillar morphology makes it very difficult to carry out a qualitative or quantitative comparison of the particle size of the MFBs with or without different compatibilizer contents.

On the other hand, and as expected, the unstretched filaments in the UBs exhibited the typical sea-island morphology of immiscible blends, with isolated domains of the minor component dispersed in a continuous phase of the main component (Figure 2a−c). Spherical and elliptical PP particles were observed without any orientation, uniformly distributed in the main LDPE matrix.

The results of average particle sizes for the UB samples are displayed in Table 1. The D values indicate a wide distribution of particle sizes as they differ from 1. The particle size was slightly affected by the amount of interfacial modifier probably because it was located at the interface, thus reducing the interfacial tension. As a result, an increase in the amount of compatibilizer slightly reduced the size of the dispersed particles.[35,41] Given the reduced size of the particles in each of the three cases (which may be responsible for the limited changes caused when the compatibilizer was added), it can be concluded that the selected blend compositions and the processing parameters used to extrude the blends effectively produced a fine dispersion of the minor component.

Table 1. Statistical Morphology Characterization

blend	d_n (μm)	d_v (μm)	D	$N \times 10^{-12}$ (cm^{-3})
UB-0	0.261	0.383	1.469	21.9
UB-7	0.253	0.384	1.515	23.9
UB-15	0.251	0.354	1.409	24.5

https://doi.org/10.1021/acsapm.1c01932
ACS Appl. Polym. Mater. XXXX, XXX, XXX−XXX

3.2. Thermal Characterization. Figure 3 shows DSC first heating scans for the blends after each step of the microfibrillation process. Figure 3a,b shows, respectively, the DSC scans of the samples after the extrusion and stretching stages, and Figure 3c shows those of the unstretched blends and stretched fibrillar compounds after injection molding (second heating scans are also indicated using dotted lines). Neat LDPE and PP have also been included as a reference. The calorimetric parameters extracted from Figure 3c are presented in Table 2.

As can be seen in Figure 3, all of the materials have two melting points at approximately 114 and 169 °C, which correspond to the LDPE and PP crystalline phases. As can also be seen, the melting peak of PP becomes broader after the second processing stage (Figure 3b) indicating a wider lamellar size distribution. This is probably a consequence of the hot stretching process.

As shown in Figure 3c, in the first DSC heating scans after the injection molding process, the PP melting endotherms of microfibrillated compounds become even broader, covering a more extensive temperature range, and display a bimodal character in most cases. This is due to a reorganization process that occurred during the DSC heating scan (i.e., melting-recrystallization-melting)[49] possibly triggered by the highly oriented crystals within the MFCs.[46,50] The microfibrillation process generates a wider distribution of oriented crystals that easily undergo relaxation, melting, and recrystallization during heating, as observed in the first heating scans of Figure 3c. After the samples melt, the thermal history is erased. The samples were cooled from the melt in the DSC at 20 °C/min where they crystallized from an isotropic melt. The second DSC heating scans (dotted lines in Figure 3c) show that the melting endotherms corresponding to the PP crystals are in general narrower and unimodal. These second heating DSC scans results (for the PP phase) thus confirm that the peculiar bimodality and broadness of the DSC first heating scans are related to the microfibrillation process and the morphological transformation that occurs upon heating the PP crystals.

With respect to the LDPE crystalline phase, the melting temperatures varied slightly (within 1−2 °C) in the drawn and injected blends compared to neat LDPE, but did not present a consistent trend. Moreover, the crystallinity of the LDPE phase decreased, compared to that of neat LDPE (included in Table 2 as a reference). The reason for this behavior is unknown, but may be related to the fibrillar morphology and the fact that the material crystallizes in the presence of solidified PP fibrils, possibly exerting a confinement effect.

The effect of the amount of compatibilizer and the stretching process on the crystallinity can also be observed in Table 2. The blends with 15 wt % of compatibilizer showed a reduction in the crystallinity of both phases, possibly caused by greater interaction between the two components. Taking into account that crystallinity determinations by DSC can yield up to 15% errors (due to the combined effects of calibration errors, baseline fluctuations, and, above all, integration errors), no significant difference in the degree of crystallinity in the PP phase was detected when the droplets were compared (UBs) with the microfibers (MFCs).

3.3. Uniaxial Tensile Behavior. Typical uniaxial stress−strain curves under quasi-static loading conditions are shown in Figure 4. As can be seen, all of the materials displayed ductile behavior after elastic deformation, with failure taking place during the necking of the specimens.

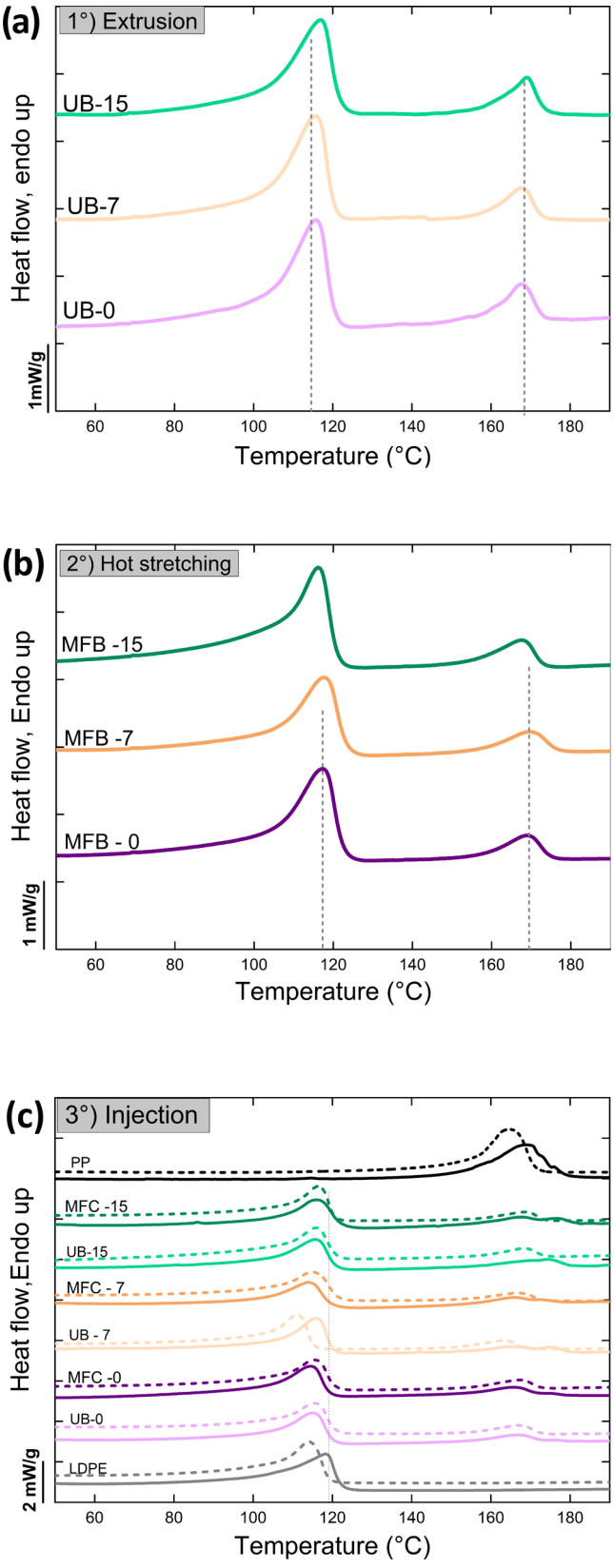

Figure 3. DSC first heating scans for each step of the microfibrillation process (a) after extrusion, (b) after stretching, and (c) after injection moulding (dotted lines indicate the melting endotherms from the second heating scans).

Table 3 shows the tensile parameters of the UB and MFC materials. On the one hand, it can be observed that the

https://doi.org/10.1021/acsapm.1c01932
ACS Appl. Polym. Mater. XXXX, XXX, XXX−XXX

Table 2. Calorimetric Parameters of the PP and LDPE Phases in UBs and MFCs after Injection Molding[a,b,c]

	LDPE							PP						
sample	T_m^1 (°C)	ΔH_m^1 (J/g)	X_c^1	ΔH_c (J/g)	T_m^2 (°C)	ΔH_m^2 (J/g)	X_c^2	T_m^1 (°C)	ΔH_m^1 (J/g)	X_c^1	ΔH_c (J/g)	T_m^2 (°C)	ΔH_m^2 (J/g)	X_c^2
UB-0	116	69	29	72	115	76	33	174	15	36	94	167	14	33
MFC-0	115	75	32	72	115	80	34	170	14	34	94	166	12	29
UB-7	114	61	26	81	114	69	29	162	14	33	95	166	15	37
MFC-7	118	75	32	78	116	52	22	162	13	27	93	169	1	27
UB-15	116	68	29	79	115	52	22	170	12	28	94	167	12	28
MFC-15	115	68	29	79	115	53	22	167	12	29	94	167	11	27

[a]1-First heating scan. [b]2-Second heating scan. [c]T_m = melting temperature, ΔH_m = measured melting enthalpy, X_c = percentage crystallinity, ΔH_c = measured crystallization enthalpy.

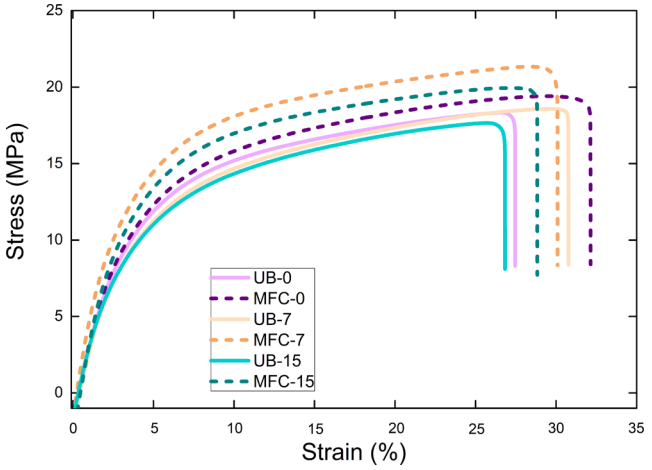

Figure 4. Stress−strain curves for the UB and MFC blends.

addition of the compatibilizer did not significantly affect the tensile behavior of the unstretched blends, which showed very similar modulus, tensile strength, and elongation at break values.

Regarding the MFC specimens, significant improvements in tensile properties were observed as a result of two overlaid effects: the stretching process and the compatibilization. It is evident that fibrillated domains of PP strengthened the LDPE matrix compared to the spherical domains of PP present in the unstretched blends. Both the tensile strength and the modulus increased significantly due to the transformation of the blends into microfibrillated composites. In addition, the PP fibers managed to reinforce the blends without any loss of ductility: the elongation at break values remained unaltered compared to those of the unstretched materials. Moreover, the compatibilization of the microfibrillated composites led to a greater increase in small-strain tensile parameters (modulus and strength), again without any loss in ductility.

Despite the fact that the MFCs presented a lower percentage of crystallinity in the LDPE phase, the improvement in mechanical behavior can be attributed to an increased load transfer between the more rigid PP and the softer LDPE due to greater interfacial interaction, which was achieved thanks to two synergistic contributions. On the one hand, the microfibers increased the contact area between the LDPE and the PP; while on the other, the presence of the compatibilizer increased the compatibility and, as a result, facilitated the stress transfer between the matrix and the fibers. The compatibilizing effect seems to be significant up to a 7 wt % compatibilizer content but diminishes once this amount is exceeded.

It has been reported that in compatibilized PP/PET microfibrillated composites, the aspect ratio of microfibrils and mechanical properties improves only up to an optimum amount, above which the properties are not only not enhanced, but are actually diminished.[39,51,52]

3.4. Fracture Behavior. All of the materials in this study exhibited ductile fracture under the applied test conditions. As can be seen in Figure 5, a well-defined maximum followed by a gradual drop in load was observed in the load−displacement curves of all of the materials. Initially, the load increases with displacement, then the ligament begins to yield, and the crack grows steadily. It was also observed that the longer the ligament, the greater the displacement and the load. The specimens exhibited a plastic zone with strain softening, indicating that the energy dissipation mechanisms were probably cavitation and matrix cracking. However, some differences between the UBs and the MFCs were observed. In the case of the MFCs (with or without a compatibilizer), as the displacement increased, the load decreased more gradually from the peak than in the case of the UBs.

The fracture behavior of the UBs and the MFCs was characterized using the EWF method, with energy partition between yielding and post-yielding. Values for the specific work of yielding ($w_{f,y}$) for all of the materials were determined by integrating the areas under the load−displacement curves up to the maximum load. Figure 6 shows the specific yielding work as a function of the ligament together with a linear fit. The resistance to the initiation of crack propagation is

Table 3. Mechanical Parameters of the UB and MFC Blends

	tensile behavior			fracture behavior		impact behavior
sample	E (MPa)	σ_{max} (MPa)	ε_b (%)	$w_{e,y}$ (kJ/m^2)	$\beta w_{p,y}$ (MJ/m^3)	impact energy (J/m)
UB-0	483 ± 5	18.6 ± 0.3	32 ± 3	0.5 ± 0.4	0.7 ± 0.1	98 ± 4
MFC-0	519 ± 11	19.5 ± 0.4	35 ± 2	2.0 ± 0.6	0.8 ± 0.1	121 ± 4
UB-7	499 ± 10	18.5 ± 0.2	32 ± 2	1.5 ± 1.0	0.7 ± 0.1	102 ± 7
MFC-7	619 ± 13	21 ± 0.4	35 ± 4	7.2 ± 1.7	0.8 ± 0.3	137 ± 10
UB-15	485 ± 6	18.3 ± 0.4	29 ± 2	2.4 ± 0.9	0.5 ± 0.1	97 ± 4
MFC-15	636 ± 19	21 ± 1	34 ± 4	6.8 ± 1.9	0.7 ± 0.2	139 ± 10

https://doi.org/10.1021/acsapm.1c01932
ACS Appl. Polym. Mater. XXXX, XXX, XXX−XXX

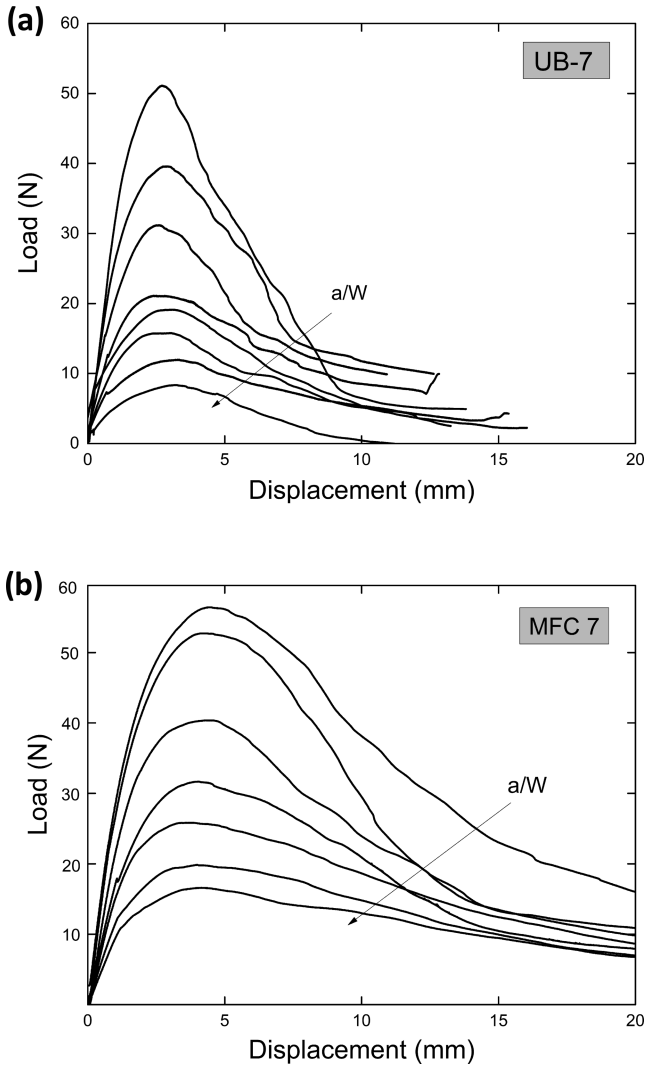

Figure 5. Load−displacement curves for (a) UB-7 and (b) MFC-7 for different ligament lengths.

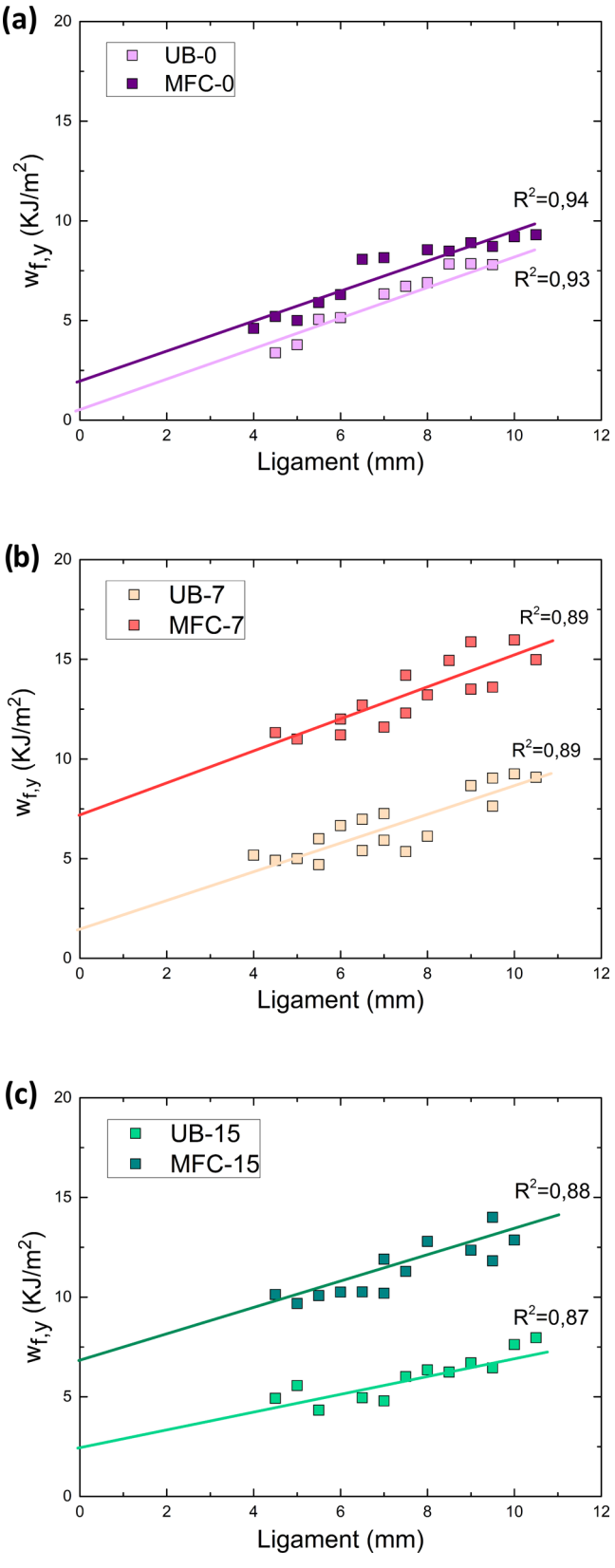

Figure 6. Work of fracture vs ligament length plots comparing UBs and MFCs. (a) Noncompatibilized, (b) with 7% compatibilizer, and (c) with 15% compatibilizer.

represented by the specific essential work of yielding ($w_{e,y}$), and the resistance to further crack propagation is related to the slope of the linear regression of $w_{f,y}$ vs L ($\beta w_{p,y}$). Table 3 shows the fracture parameters from the EWF analysis.

Regarding the unstretched blends, a slight increase in the initiation parameter values ($w_{e,y}$) was observed when a compatibilizer was added, while the propagation parameter remained constant. This is attributed to the high degree of incompatibility between the LDPE and PP phases as well as the stress-concentrating effect of the PP particles, which both make it easier to create a path for crack propagation.[47,48]

Regarding the microfibrillated composites, compared to the UBs, a significant increase in the initiation parameter value ($w_{e,y}$) was observed when no compatibilizer was added. In fact, this increase was even higher in the case of compatibilized blends. According to Mai and co-authors,[53] in short glass fiber-reinforced thermoplastics, the physical meaning of $w_{e,y}$ is the work required to debond, slide and pull out the fibers, deform the matrix, and subsequently fracture it through the crack plane in the fracture process zone. In the MFC samples presented here, the injection process was performed above the melting temperature of the matrix component (LDPE), but below that of the second phase (PP), with a view to preserving the PP microfibers in the final pieces. Consequently, the PP microfibers were in a solid state during this processing step. As the blend cooled from processing to room temperature

https://doi.org/10.1021/acsapm.1c01932
ACS Appl. Polym. Mater. XXXX, XXX, XXX−XXX

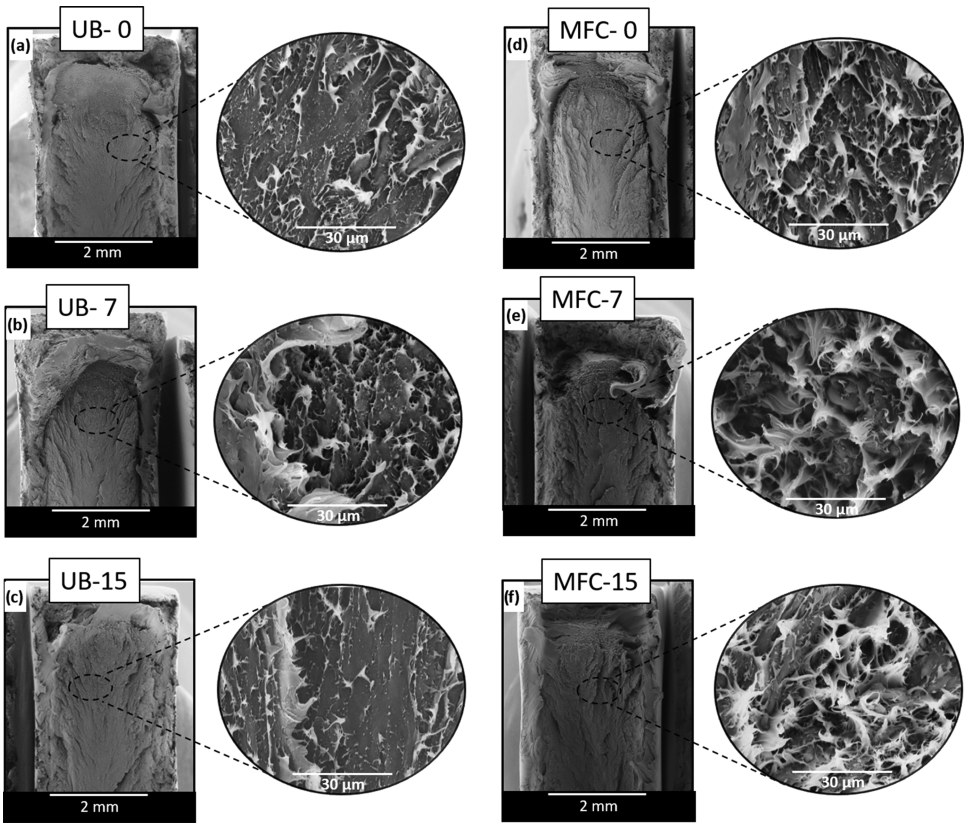

Figure 7. SEM micrographs of the Izod impact test fracture surfaces of the UBs and the MFCs: UB-0 (a), UB-7 (b), UB-15 (c), MFC-0 (d), MFC-7 (e), MFC-15 (f).

inside the mold, the LDPE experienced crystallization shrinkage, while the PP microfibers hardly shrank due to the absence of phase transition, i.e., only molecular relaxation occurred. Therefore, high thermal residual stress (compressive stress) developed between the PP fibers and the LDPE matrix. During testing, due to the deformation of the matrix, relative motion at the interfaces was favored and thus, a frictional force was generated. The frictional force caused the PP fibers to withstand the external stress and consequently strengthened the final sample. This effect was amplified in the presence of the compatibilizer, probably due to the increased fiber/matrix interaction.[53,54]

Regarding the propagation stage, the nonessential work $\beta w_{p,y}$ remained constant as the compatibilizer content increased, both in the UB and the MFC samples. This parameter indicates the energy required for plastic deformation to occur mainly in the LDPE matrix. This result is probably due to the excess of microfibers in the matrix (indicated by the large number of particles observed in the blends before stretching), which limits the ductility of the samples. This is because the microfibers themselves have a low capacity for deformation, and the interfacial adhesion between the fibers and the LDPE was poor due to their incompatibility,[54] even at large compatibilizer contents.

3.5. Behavior under Impact Conditions. The impact energy values obtained by noninstrumented Izod tests for all of the studied materials are shown in Table 3. The MFCs presented significantly higher impact resistance values than the corresponding unstretched blends (23, 34, and 43% with respect to 0, 7, and 15% compatibilized materials, respectively). As for the tensile behavior previously explained, the fibrillated morphology of the dispersed phase (PP) allowed a greater load transfer on impact, possibly due to the greater contact surface area between the PP fibers and the LDPE matrix. Actually, the toughness calculated from the stress−strain curves of the tensile test showed similar results (16, 25, and 39% increases with respect to unstretched blends) to those of Izod impact test. With respect to the effect of compatibilization, barely significant increases were observed in the UBs. However, a 13% increase in the impact strength was observed in the 7% compatibilized MFC compared to the noncompatibilized MFC, with no further increases detected at higher compatibilizer contents, consistent with the results reported by Zanjanijam et al.[55] for PP/PVB blends. The favorable behavior of the compatibilized MFCs can be attributed to an increase in the interfacial adhesion, which led to a more efficient stress transfer between the PP fibrillar domains.[56] These results contrast with those reported in the literature[35,36] for LDPE/PET blends compatibilized with graft copolymers where compatibilized MFCs showed a decrease in impact energy compared to noncompatibilized MFCs. The authors attributed their observations to the amount of compatibilizer added, which caused a discontinuity in the PET microfibers, which further deteriorated during the isotropization process.

The fracture surfaces of the specimens subjected to the Izod impact tests are presented in Figure 7. The toughness of polymeric materials can usually be easily related to the roughness observed in SEM micrographs: a rough fracture surface indicates a ductile material with high impact resistance. It was observed that the UB-0 samples presented smoother fracture surfaces than the corresponding MFC-0 samples,

https://doi.org/10.1021/acsapm.1c01932
ACS Appl. Polym. Mater. XXXX, XXX, XXX−XXX

confirming that the microfibrillation process promoted plastic deformation even during impact fracture and therefore energy absorption. The surfaces of the compatibilized blends (UB-7 and UB-15) were similar to the noncompatibilized UB-0, exhibiting smoother fracture surfaces than the MFC samples. A higher degree of plastic deformation was achieved in MFC-7 and MFC-15, in comparison with MFC-0; the fracture surfaces were rougher and the ductile tearing deformation mechanisms were greater in the first two than in the MFC-0 samples. As previously mentioned, the addition of the compatibilizer and the microfibrillation process have a synergistic effect on the damage mechanism which was clearly evidenced in the impact toughness values.

4. CONCLUSIONS

In this work, the improvement of the mechanical performance of LDPE/PP blends through morphology manipulation was analyzed. It was possible to obtain microfibrillated composites by in situ formation and development of PP microfibrils in an LDPE matrix following an unusual combination of common industrial processing techniques. Both nonstretched blends (UBs) and microfibrillar composites (MFCs) were studied at varying compatibilizer concentrations of 0, 1.4, and 3 wt % of the total PE/PP content (0, 7, and 15 wt % of the minority phase).

The morphologies of the UBs and the MFCs were analyzed at different processing stages. As expected, the UB samples exhibited a droplet morphology. The MFCs presented a fibrillar morphology, which could be verified indirectly by analyzing their mechanical behavior.

The tensile strength of the MFCs increased by 15% compared with the UBs, regardless of the amount of compatibilizer added. Young's modulus increased by a higher percentage (from 7 to 30%) when the compatibilizer was added. Furthermore, this reinforcing effect occurred without any loss of high-strain mechanical properties, i.e., elongation at break. No further significant changes in tensile properties were found when the compatibilizer content was increased.

Fracture characterization by the EWF showed that the resistance to the initiation of fracture propagation increased in the MFCs relative to the UBs. This parameter showed a dependence on the morphology of the dispersed phase (particulate vs microfibrillated) and on the presence of the compatibilizer. From these results, it is evident that the incorporation of PP microfibrils in the LDPE matrix allows a significant improvement in fracture toughness.

Finally, the microfibrillation process in the LDPE/PP blends led to a 23% increase in the impact resistance relative to the unstretched blends. This parameter was further increased (to 43%) when a compatibilizer was added. Again, no significant differences were found when the compatibilizer content was increased.

As it was said before, a circular economy requires new technologies for the treatment of waste. Based on our results, it is evident that this type of processing has enormous potential for large-scale application in immiscible recycled polyolefin blends where final properties can be improved by modifying their morphology. The application of these conventional processing techniques in a nonconventional way is innovative and represents a significant and positive contribution to the recycling of the world's top two polymers through simple melt blending, as the process could be easily used in a production environment, obviating the need to separate these plastics in mixed waste streams.

AUTHOR INFORMATION

Corresponding Author

Gonzalo Guerrica-Echevarría − *POLYMAT and Department of Advanced Polymers and Materials: Physics, Chemistry and Technology, Faculty of Chemistry, University of the Basque Country UPV/EHU, 20018 Donostia-San Sebastian, Spain;* orcid.org/0000-0003-1255-8899; Email: gonzalo.gerrika@ehu.eus

Authors

Caren Rosales − *INTEMA, University of Mar Del Plata—CONICET, 7600 Mar Del Plata, Argentina;* orcid.org/0000-0002-1942-5354

Nora Aranburu − *POLYMAT and Department of Advanced Polymers and Materials: Physics, Chemistry and Technology, Faculty of Chemistry, University of the Basque Country UPV/EHU, 20018 Donostia-San Sebastian, Spain;* orcid.org/0000-0001-5730-9867

Itziar Otaegi − *POLYMAT and Department of Advanced Polymers and Materials: Physics, Chemistry and Technology, Faculty of Chemistry, University of the Basque Country UPV/EHU, 20018 Donostia-San Sebastian, Spain;* orcid.org/0000-0001-8269-8489

Valeria Pettarin − *INTEMA, University of Mar Del Plata—CONICET, 7600 Mar Del Plata, Argentina;* orcid.org/0000-0001-7927-2647

Celina Bernal − *ITPN, University of Buenos Aires—CONICET, 1127 Buenos Aires, Argentina;* orcid.org/0000-0002-6949-3400

Alejandro J. Müller − *POLYMAT and Department of Advanced Polymers and Materials: Physics, Chemistry and Technology, Faculty of Chemistry, University of the Basque Country UPV/EHU, 20018 Donostia-San Sebastian, Spain; IKERBASQUE, Basque Foundation for Science, 48009 Bilbao, Spain;* orcid.org/0000-0001-7009-7715

Complete contact information is available at: https://pubs.acs.org/10.1021/acsapm.1c01932

Funding

This research was funded by Ministerio de Ciencia, Tecnología e Innovación Productiva - Agencia Nacional de Promoción Científica y Tecnológica (Project PICT 2015-2032), Consejo Nacional de Investigaciones Científicas y Técnicas (predoctoral grant awarded to Caren Rosales), and Eusko Jaurlaritza (Project IT1309-19).

Notes

The authors declare no competing financial interest.

REFERENCES

(1) UNITED NATIONS ENVIRONMENT PROGRAMME *Single-Use Plastics: A Roadmap for Sustainability*; UNEP, 2018; 15−978-92-807-3705-9. https://www.unep.org/resources/report/single-use-plastics-roadmap-sustainability.

(2) Geissdoerfer, M.; Savaget, P.; Bocken, N.; Hultink, E. The Circular Economy − A new sustainability paradigm. *J. Cleaner Prod.* **2017**, *143*, 757−768.

(3) Korhonen, J.; Honkasalo, A.; Seppälä, J. Circular Economy: The Concept and its Limitations. *Ecol. Econ.* **2018**, *143*, 37−46.

(4) Lett, L. Las amenazas globales, el reciclaje de residuos y el concepto de economía circular. *Rev. Argent. Microbiol.* **2014**, *41*, 1−2.

https://doi.org/10.1021/acsapm.1c01932
ACS Appl. Polym. Mater. XXXX, XXX, XXX−XXX

(5) Ragaert, K.; Huysveld, S.; Vyncke, G.; Hubo, S.; Veelaert, L.; Dewulf, J.; Du Bois, E. Design from recycling: A complex mixed plastic waste case study. *Resour., Conserv. Recycl.* **2020**, *155*, No. 104646.
(6) Foundation TEM. Circular Economy - UK, USA, Europe, Asia & South America, 2019, https://www.ellenmacarthurfoundation.org.
(7) Jubinville, D.; Esmizadeh, E.; Saikrishnan, S.; Tzoganakis, C.; Mekonnen, T. A comprehensive review of global production and recycling methods of polyolefin (PO) based products and their post-recycling applications. *Sustainable Mater. Technol.* **2020**, *25*, No. e00188.
(8) Wang, H.; Zhang, Y.; Wang, C. Surface modification and selective flotation of waste plastics for effective recycling: a review. *Sep. Purif. Technol.* **2019**, *226*, 75−94.
(9) Jose, S.; Aprem, A. S.; Francis, B.; Chandy, M. C.; Werner, P.; Alstaedt, V.; Thomas, S. Phase morphology, crystallisation behaviour and mechanical properties of isotactic polypropylene / high density polyethylene blends. *Eur. Polym. J.* **2004**, *40*, 2105−2115.
(10) Mourad, A.-H. I.; Akkad, R. O.; Soliman, A. A.; Madkour, T. M. Characterisation of thermally treated and untreated polyethylene−polypropylene blends using DSC, TGA and IR techniques. *Plast., Rubber Compos.* **2009**, *38*, 265−278.
(11) Salih, S. E.; Hamood, A. F.; Abd alsalam, A. H. Comparison of the characteristics of LDPE: PP and HDPE: PP polymer blends. *Mod. Appl. Sci.* **2013**, *7*, 33−42.
(12) Fang, C.; Nie, L.; Liu, S.; Yu, R.; An, N.; Li, S. Characterization of polypropylene-polyethylene blends made of waste materials with compatibilizer and nano-filler. *Compos. B. Eng.* **2013**, *55*, 498−505.
(13) Guerfi, N.; Bensemra, N. Preparation, characterization and valorization of regenerated low density polyethylene/polypropylene blends. *Environ. Eng. Manage. J.* **2014**, *13*, 2609−2613.
(14) Borovanska, I.; Dobreva, T.; Benavente, R.; Djoumaliisky, S.; Kotzev, G. Quality assessment of recycled and modified LDPE / PP blends. *J. Elastomers Plast.* **2012**, *44*, 479−497.
(15) Penava, N. V.; Rek, V.; Slouf, M.; Jelcic, Z. Influence of ethylene-propylene-diene terpolymer addition on processing parameters, phase structure and thermal behaviour of polypropylene/low-density polyethylene blends. *J. Elastomers Plast.* **2015**, *47*, 502−514.
(16) Clemons, C. Elastomer modified polypropylene-polyethylene blends as matrices for wood flour-plastic composites. *Composites, Part A* **2010**, *41*, 1559−1569.
(17) Radonjič, G.; Gubeljak, N. The use of ethylene/propylene copolymers as compatibilizers for recycled polyolefin blends. *Macromol. Mater. Eng.* **2002**, *287*, 122−132.
(18) Yang, M.; Wang, K.; Ye, L.; Mai, Y.-W.; Wu, J. Low density polyethylene-polypropylene blends Part 2 - Strengthening and toughening with copolymer. *Plast., Rubber Compos.* **2003**, *32*, 27−31.
(19) Mourad, A.-H. I. Thermo-mechanical characteristics of thermally aged polyethylene/polypropylene blends. *Mater. Des.* **2010**, *31*, 918−929.
(20) Dhoble, A.; Kulshreshtha, B.; Ramaswami, S.; Zumbrunnen, D. A. Mechanical properties of PP-LDPE blends with novel morphologies produced with a continuous chaotic advection blender. *Polymer* **2005**, *46*, 2244−2256.
(21) Jin, M.; Jin, B.; Xu, X.; Li, X.; Wang, T.; Zhang, J. Effects of ultrahigh molecular weight polyethylene and mould temperature on morphological evolution of isotactic polypropylene at micro-injection moulding condition. *Polym. Test.* **2015**, *46*, 41−49.
(22) Shan, G.-F.; Yang, W.; Xie, B.-H.; Yang, M.-B. Mechanical properties and morphology of LDPE/PP blends. *J. Macromol. Sci., Part B: Phys.* **2007**, *46*, 963−974.
(23) Shanks, R. A.; Li, J.; Yu, L. Polypropylene-polyethylene blend morphology controlled by time-temperature-miscibility. *Polymer* **2000**, *41*, 2133−2139.
(24) Wong, A. C.-Y. Heat deflection characteristics of polypropylene and polypropylene/polyethylene binary systems. *Composites, Part B* **2003**, *34*, 199−208.
(25) Wu, T.; Li, Y.; Wu, G. Crystalline structure and phase structure of mLLDPE/LDPE blends. *Polymer* **2005**, *46*, 3472−3480.
(26) Rosales, C.; Brendstrup, D.; Bernal, C.; Pettarin, V. Morphology/tensile performance relationship for LLDPE/PP double gated injected blends. *Adv. Mater. Lett.* **2020**, *11*, 1−6.
(27) Rosales, C.; Bernal, C.; Pettarin, V. Effect of blend composition and related morphology on the quasi-static fracture performance of LLDPE/PP blends. *Polym. Test.* **2020**, *90*, No. 106598.
(28) Xu, J.; Eagan, J. M.; Kim, S.-S.; Pan, S.; Lee, B.; Klimovica, K.; Jin, K.; Lin, T.-W.; Howard, M. J.; Ellison, C. J.; LaPointe, A. M.; Coates, G. W.; Bates, F. S. Compatibilization of Isotactic Polypropylene (iPP) and High-Density Polyethylene (HDPE) with iPP−PE Multiblock Copolymers. *Macromolecules* **2018**, *51*, 8585−8596.
(29) Mishra, R. K.; Thomas, S.; Kalarikkal, N. *Micro and Nano Fibrillar Composites from Polymer Blends*; Woodhead Publishing, 2017; pp 233−258.
(30) Kuzmanović, M.; Delva, L.; Cardon, L.; Ragaert, K. Relationship between the Processing, Structure, and Properties of Microfibrillar Composites. *Adv. Mater.* **2020**, *52*, 1−29.
(31) Yi, X.; Xu, L.; Wang, Y.-L.; Zhong, G.-J.; Ji, X.; Li, Z.-M. Morphology and properties of isotactic polypropylene/poly(ethylene terephthalate) in situ microfibrillar reinforced blends: Influence of viscosity ratio. *Eur. Polym. J.* **2010**, *46*, 719−730.
(32) Jayanarayanan, K.; Jose, T.; Thomas, S.; Joseph, K. Effect of draw ratio on the microstructure, thermal, tensile and dynamic rheological properties of in situ microfibrillar composites. *Eur. Polym J.* **2009**, *45*, 1738−1747.
(33) Jayanarayanan, K.; Thomas, S.; Joseph, K. In situ microfibrillar blends and composites of polypropylene and poly (ethylene terephthalate): Morphology and thermal properties. *J. Polym. Res.* **2011**, *18*, 1−11.
(34) Mi, D.; Wang, Y.; Kuzmanovic, M.; Delva, L.; Jiang, Y.; Cardon, L.; Zhang, J.; Ragaert, K. Effects of phase morphology on mechanical properties: Oriented/unoriented PP crystal combination with spherical/microfibrillar PET phase. *Polymers* **2019**, *11*, No. 248.
(35) Jayanarayanan, K.; Ravichandran, A.; Rajendran, D.; Sivathanupillai, M.; Venkatesan, A.; Thomas, S.; Joseph, K. Morphology and Mechanical Properties of Normal Blends and In-Situ Microfibrillar Composites from Low-Density Polyethylene and Poly(ethylene terephthalate). *Polym.-Plast. Technol. Eng.* **2010**, *49*, 442−448.
(36) Jayanarayanan, K.; Thomas, S.; Joseph, K. Effect of blend ratio on the mechanical and sorption behaviour of polymer-polymer microfibrillar composites from low-density polyethylene and poly-ethylene terephthalate. *J. Reinf. Plast. Compos.* **2012**, *31*, 549−562.
(37) Fakirov, S.; Kamo, H.; Evstatiev, M.; Friedrich, K. Microfibrillar reinforced composites from PET/LDPE blends: Morphology and mechanical properties. *J. Macromol. Sci., Part B* **2004**, *43*, 775−789.
(38) Kuzmanović, M.; Delva, L.; Mi, D.; Martins, C. I.; Cardon, L.; Ragaert, K. Development of crystalline morphology and its relationship with mechanical properties of PP/PET microfibrillar composites containing POE and POE-g-MA. *Polymers* **2018**, *10*, 291.
(39) Taepaiboon, P.; Junkasem, J.; Dangtungee, R.; Amornsakchai, T.; Supaphol, P. In situ microfibrillar-reinforced composites of isotactic polypropylene/recycled poly(ethylene terephthalate) system and effect of compatibilizers. *J. Appl. Polym. Sci.* **2006**, *102*, 1173−1189.
(40) Li, W.; Schlarb, A. K.; Evstatiev, M. Influence of Processing Window and Weight Ratio on the Morphology of the Extruded and Drawn PET/PP Blends. *Acta Med. Okayama* **2016**, *70*, 111−118.
(41) Arnal, M. L.; Matos, M. E.; Morales, R. A.; Santana, O. O.; Müller, A. J. Evaluation of the fractionated crystallization of dispersed polyolefins in a polystyrene matrix. *Macromol. Chem. Phys.* **1998**, *199*, 2275−2288.
(42) Jayanarayanan, K.; Bhagawan, S. S.; Thomas, S.; Joseph, K. Morphology development and non isothermal crystallization behaviour of drawn blends and microfibrillar composites from PP and PET. *Polym. Bull.* **2008**, *60*, 525−532.
(43) Martinez, A. B.; Gamez-Perez, J.; Sanchez-Soto, M.; Velasco, J. I.; Santana, O. O.; Maspoch, M. Ll. The Essential Work of Fracture

https://doi.org/10.1021/acsapm.1c01932
ACS Appl. Polym. Mater. XXXX, XXX, XXX−XXX

(EWF) method - Analyzing the Post-Yielding Fracture Mechanics of polymers. *Eng. Failuer Anal.* **2009**, *16*, 2604−2617.
(44) Karger-Kocsis, J. Microstructural and molecular dependence of the work of fracture parameters in semicrystalline and amorphous polymer systems. *Eur. Struct. Integr. Soc. Publ. EGF/ESIS Publ.* **2000**, *27*, 213−230.
(45) Ferrer-Balas, D.; Maspoch, M. Ll.; Martinez, A. B.; Santana, O. O. On the essential work of fracture method: Energy partitioning of the fracture process in iPP films. *Polym. Bull.* **1999**, *42*, 101−108.
(46) Monasse, B.; Haudin, J. M. Effect of random copolymerization on growth transition and morphology change in polypropylene. *Colloid Polym. Sci.* **1988**, *266*, 679−687.
(47) Harrats, C.; Thomas, S.; Groeninckx, G. Micro- and Nanostructured Multiphase Polymer Blend Systems. *Taylor & Francis Group* **2006**, 207−230.
(48) Haghnegahdar, M.; Naderi, G.; Ghoreishy, M. H. R. Fracture toughness and deformation mechanism of un-vulcanized and dynamically vulcanized polypropylene/ethylene propylene diene monomer/graphene nanocomposites. *Compos. Sci. Technol.* **2017**, *141*, 83−98.
(49) Varga, J. Supermolecular structure of isotactic polypropylene. *J. Mater. Sci.* **1992**, *27*, 2557−2579.
(50) Monasse, B.; Haudin, J. M. Growth transition and morphology change in polypropylene. *Colloid Polym. Sci.* **1985**, *263*, 822−831.
(51) Rybnikar, F.; Kaszonyiova, M. Epitaxial crystallization of linear polyethylene in blends with isotactic polypropylene. *J. Macromol. Sci., Part B* **2014**, *53*, 217−232.
(52) Friedrich, K.; Evstatiev, M.; Fakirov, S.; Evstatiev, O.; Ishii, M.; Harrass, M. Microfibrillar reinforced composites from PET/PP blends: processing, morphology and mechanical properties. *Compos. Sci. Technol.* **2005**, *65*, 107−116.
(53) Mai, Y. W.; Wong, S. C.; Chen, X. H. Application of Fracture Mechanics for Characterization of Toughness of Polymer Blends. Paul, D. R.; C, B. B., Eds.; Wiley & Sons, 2000; pp 1−17.
(54) Li, Z.-M.; Yang, W.; Huang, R.; Fang, X.-P.; Yang, M.-B. Essential work of fracture parameters of in-situ microfibrillar poly(ethylene terephthalate)/polyethylene blend: Influences of blend composition. *Macromol. Mater. Eng.* **2004**, *289*, 426−433.
(55) Zanjanijam, A. R.; Hakim, S.; Azizi, H. Morphological, dynamic mechanical, rheological and impact strength properties of the PP/PVB blends: The effect of waste PVB as a toughener. *RSC Adv.* **2016**, *6*, 44673−44686.
(56) Mao, Z.; Zhang, X.; Jiang, G.; Zhang, J. Fabricating sea-island structure and co-continuous structure in PMMA/ASA and PMMA/CPE blends: Correlation between impact property and phase morphology. *Polym. Test.* **2019**, *73*, 21−30.

https://doi.org/10.1021/acsapm.1c01932
ACS Appl. Polym. Mater. XXXX, XXX, XXX−XXX